

NANO EXPRESS

Open Access



Two-Solvent Method Synthesis of NiO/ZnO Nanoparticles Embedded in Mesoporous SBA-15: Photocatalytic Properties Study

Peng Dai^{1*}, Tao-tao Yan¹, Xin-xin Yu¹, Zhi-man Bai¹ and Ming-zai Wu^{1,2*}

Abstract

Different loadings of NiO/ZnO nanoparticles embedded in mesoporous silica (SBA-15) were prepared via a two-solvent method with the ordered hexagonal mesoporous structure of SBA-15 kept. X-ray diffraction, transmission electron microscope, X-ray photoelectron spectroscopy, diffusive reflective UV-vis spectroscopy, and N₂ adsorption porosimetry were employed to characterize the nanocomposites. The results indicate that the ordered hexagonal mesoporous structure of SBA-15 is kept and the absorption band edges of the nanocomposites shift into the ultraviolet light regime. The photocatalytic activity of our samples for degradation of methylene orange was investigated under UV light irradiation, and the results show that the nanocomposites have higher photodegradation ability toward methylene orange than commercial pure P-25. The photocatalytic activity of the nanocomposites was found to be dependent on both the adsorption ability of the SBA-15 and the photocatalytic activity of NiO-ZnO nanoparticles encapsulated in SBA-15. In addition, there is an optimal loading of NiO-ZnO nanoparticles. Too high or low loading will lower the photodegradation ability of the nanocomposites.

Keywords: Mesoporous silica, Nanocomposites, Photocatalysis, Two-solvent method

Background

Over the past two decades, semiconductor metal oxides have become the promising photocatalysts in environmental remediation for their nontoxic nature, low cost, and chemical stability [1–3]. Among these semiconductor metal oxides, zinc oxide (ZnO) has been recognized as an excellent material for photocatalytic processes for its high photosensitivity, low cost, and environmental friendliness [4–6]. However, the commercial application of ZnO is still subject to higher band gap (about 3.37 eV) and faster recombination of photogenerated electron-hole pairs. To solve these problems, great efforts have been made to enhance the photocatalytic performance of ZnO nanostructures. Recently, the preparation of ZnO-based heterojunctions including noble metal, and other selected semiconductor with regulated bands, is reported for the enhancement of photocatalytic performance, which can facilitate the mutual transfer of photogenerated electrons

and holes and help to suppress the recombination of electron and hole [7, 8]. Among these heterojunctions, NiO-ZnO heterojunctional nanostructures have received special research interest. NiO, a p-type semiconductor ($E_g = 3.5$ eV) possesses high hole concentration, high hole mobility, and low lattice mismatch with ZnO, which facilitates the formation of *p-n* heterojunction with ZnO [9, 10]. Recently, electrospun and thermal oxidization methods have been reported for the preparation of NiO-ZnO heterojunctions with enhanced photocatalytic activities [11, 12]. However, these methods are subject either to high cost equipment or nanoparticle aggregation, which increases the grain size, reduces the specific surface area, and depresses the photocatalytic activity. Therefore, the exploitation of a new way for the facile preparation of NiO-ZnO heterojunctions is still highly desired.

In this paper, a facile impregnation technique named “two-solvent” method was developed for the preparation of NiO-ZnO nanoparticles encapsulated in mesoporous SBA-15 silica. Hydrophobic alkane solvent (*n*-hexane, *n*-pentane, or cyclohexane) were first used to impregnate SBA-15 [13–15], increasing the number of germinal and

* Correspondence: daipeng@mail.ustc.edu.cn; mingzaiwu@gmail.com

¹Key laboratory of Information Materials and Device, School of Physics and Materials Science, Anhui University, Hefei 230039, People's Republic of China
Full list of author information is available at the end of the article

hydrogen bonded silanol, which can result in better wettability and facilitate the introduction of aqueous solutions into the pores. When metal precursor aqueous solution is introduced, the droplets of the solution are liable to be pushed into the pore channels of SBA-15 for the nonpolar hydrophobic environment and the hydrophilic nature of SBA-15. Thus, guest species can be confined and homogeneously distributed within the pores of SBA-15, which prevents nanoparticle aggregation. To our best knowledge, there has been no report on the preparation of NiO/ZnO nanoparticles encapsulated in SBA-15.

Methods

Synthesis of NiO/ZnO/SBA-15 Nanocomposites

All chemicals in this paper are analytical pure grade and used as received. The mesoporous silica SBA-15 was synthesized based on ref [16]. The NiO/ZnO/SBA-15 nanocomposites were fabricated by the two-solvent impregnation method at 298 K [17]. In a typical synthesis, 1 g of extracted mesoporous silica SBA-15 was added into 30 mL of *n*-hexane (hydrophobic solvent) with vigorous stirring of 2 h. Then, 0.98 mL of the mixture solution (hydrophilic solvent) of $\text{Zn}(\text{NO}_3)_2 \cdot 6\text{H}_2\text{O}$ and $\text{Ni}(\text{NO}_3)_2 \cdot 6\text{H}_2\text{O}$ with the atom ratio of Zn to Ni of 1:1 were introduced to the above mixture dropwise with vigorous stirring until a paste-like product turned up, which was dried for 12 h ambiently. Finally, NiO/ZnO/SBA-15 nanocomposites were obtained by calcining the dried product at 550 °C for 5 h in a muffle oven at a ramping rate of 1 °C/min. The NiO/ZnO/SBA-15 nanocomposites with different loading of NiO/ZnO nanoparticles are labeled as *x* % NiO/ZnO/SBA-15, where *x* shows the weight percentage of NiO and ZnO in the nanocomposites (the atom ratio of Zn to Ni is kept to be 1:1). Moreover, 30 % NiO/SBA-15 and 30 % ZnO/SBA-15 were also prepared for the comparative study of photocatalytic properties via the same procedure.

Characterization and Measurements

X-ray diffraction (XRD) patterns were collected on an 18 kW advanced X-ray diffractometer equipped with Cu K_α radiation ($\lambda = 1.54056 \text{ \AA}$). Transmission electron microscopy (TEM) patterns were obtained with JEOL JEM-2100, operating at 200 kV. Brunauer-Emmett-Teller (BET) surface and the pore structures of the samples were measured at 77 K by a micromeritics ASAP2010 nitrogen isothermal adsorption instrument. The pore volumes were determined at a P/P_0 value of 0.97, the specific surface areas were computed with the BET equation, and the mean pore diameters were calculated with the Barrett-Joyner-Halenda (BJH) method based on the adsorption branch of the N_2 isotherm curve. X-ray photoelectron spectroscopy (XPS) was performed on a PHI-5702 instrument with Al K_α radiation as the excitation source

($h\nu = 1486.7 \text{ eV}$). UV-vis absorption spectra were recorded on a shimadzu 240 UV-vis spectrophotometer.

Photocatalytic Experimental Details

The photocatalytic degradation experiments for methylene orange (MO) were carried out in a self-prepared reactor. In the degradation procedure, samples were immersed in a 50-mL beaker containing 40 mL of MO aqueous solution (20 mg/L). Before the solution was irradiated by a 350 W Xenon lamp, the vertical distance between the solution level and the horizontal plane of the lamp was fixed at 10 cm. At an interval of 10 min, 3 mL of solution was taken out from the reactor. The absorbance of the solution was determined on a UV-vis absorption photometer (UV-3200S, MAPADA analytic apparatus Ltd. Inc., Shanghai, China) at a 464-nm wavelength.

Results and Discussion

Characteristic of NiO/ZnO/SBA-15 Nanocomposites

Figure 1 shows the low-angle XRD (LAXRD) patterns of SBA-15 and the nanocomposites with various NiO/ZnO loadings. For pure SBA-15, a strong diffraction peak at 2θ of 0.83° and two weak peaks at 2θ of 1.44° and 1.67° are detected and can be well indexed to (100), (110), and (200) planes of the hexagonal space group ($P6 \text{ mm}$), suggesting good long-range order of the as-prepared SBA-15 [16]. Nanocomposites with 20, 30, and 40 % of NiO-ZnO loadings show similar diffraction peaks to SBA-15, indicating that the introduction of NiO/ZnO particles does not destroy the ordered mesoporous structure. The (100) peak at 2θ of 20 % NiO/ZnO/SBA-15, 30 % NiO/ZnO/SBA-15, and 40 % NiO/ZnO/SBA-15 are located at 0.89° , 0.87° , 0.86° , respectively. The d_{100} interplanar spacings can be calculated to be 9.9, 10.1, and 10.3 nm for 20 % NiO/ZnO/SBA-15, 30 % NiO/ZnO/SBA-15, and 40 % NiO/ZnO/SBA-15, respectively.

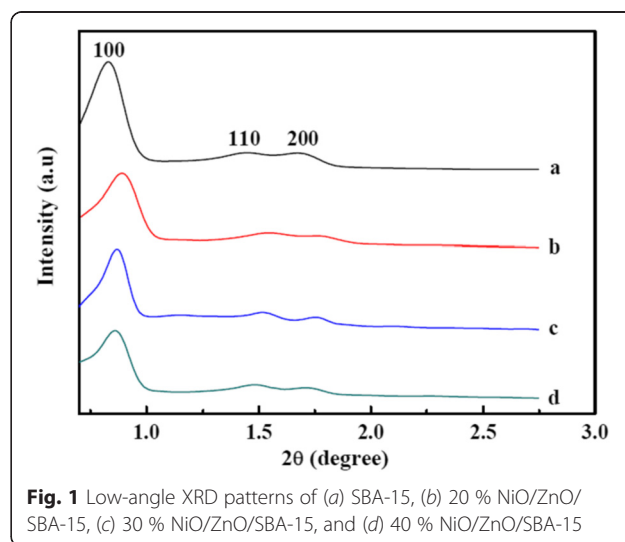


Fig. 1 Low-angle XRD patterns of (a) SBA-15, (b) 20 % NiO/ZnO/SBA-15, (c) 30 % NiO/ZnO/SBA-15, and (d) 40 % NiO/ZnO/SBA-15

Obviously, with the increase of NiO/ZnO loading, the mesoporous structure of the NiO/ZnO/SBA-15 nanocomposites expands [18]. Furthermore, based on the formula $a_0 = 2d_{100}/\sqrt{3}$, the unit cell parameter a_0 of samples 20 % NiO/ZnO/SBA-15, 30 % NiO/ZnO/SBA-15, and 40 % NiO/ZnO/SBA-15 are calculated to be 11.4, 11.7, and 11.9, respectively.

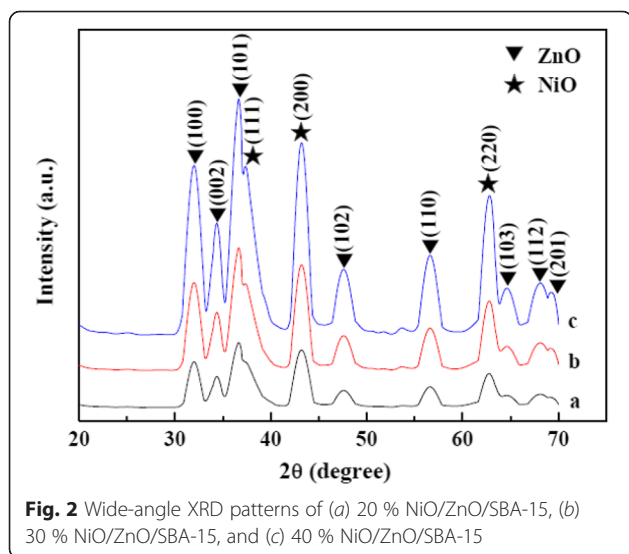
Figure 2 shows the wide-angle XRD patterns of samples 20 % NiO/ZnO/SBA-15, 30 % NiO/ZnO/SBA-15, and 40 % NiO/ZnO/SBA-15. Two sets of diffraction peaks can be indexed to cubic NiO (JCPDS card no. 78-0643) and hexagonal ZnO (JCPDS card no. 36-1451), respectively. No peaks of impurity are detected. With the increase of NiO/ZnO loading, peaks become sharper and narrower, suggesting that the crystalline of NiO/ZnO nanoparticles is improved. Based on the Scherrer equation using (200) diffraction peak of NiO, the crystalline sizes of NiO for these three samples are estimated to be 5.0, 5.4, and 5.7 nm, respectively. While for ZnO nanoparticles, the estimated crystalline sizes are 5.2, 5.7, and 6.1 nm for samples of 20 % NiO/ZnO/SBA-15, 30 % NiO/ZnO/SBA-15, and 40 % NiO/ZnO/SBA-15, respectively, using the (100) peak.

Figure 3 shows TEM images of pure SBA-15 and 30 % NiO/ZnO/SBA-15. For SBA-15, one-dimensional ordered channels are clearly observed, as shown in Fig. 3a. For 30 % NiO/ZnO/SBA-15 sample, two-dimensional hexagonal structure of the silica template is still preserved, after the loading and crystallization of NiO/ZnO with no detected large oxide particles outside the sample surface. Higher magnification image of sample 30 % NiO/ZnO/SBA-15 is shown in Fig. 3c. Clearly, NiO and ZnO nanoparticles are uniformly dispersed in the mesopores of SBA-15, as shown by the circled areas. The size

of 8 nm for NiO/ZnO particles is less than the unit cell parameter a_0 (11.7 nm) of SBA-15. Figure 3d further presents the HRTEM image of rectangular area of Fig. 3c. The interplanar distances of 0.24 and 0.26 nm are in good agreement with the lattice spacing of the (111) planes of the cubic NiO and the (002) planes of the hexagonal ZnO, respectively. Obviously, the ZnO particle and NiO particle combine together and form a heterojunction.

The chemical composition of sample 30 % NiO/ZnO/SBA-15 was studied by XPS analysis, and the corresponding results are shown in Fig. 4. The peak centered at 102.6 eV is indexed to Si 2p, which is absolutely from silica in SBA-15, as shown in Fig. 4a [19]. Figure 4b shows the O 1s XPS spectrum, which is asymmetric and abroad, indicating the existence of more than one chemical state for oxygen species. Hence, the region of O 1s was deconvoluted into two Gaussian peaks centered at 530.8 and 531.9 eV. The lower binding energy at 530.8 eV is attributed to the oxygen in NiO and ZnO [20], while the peak centered at 531.9 eV is due to the adsorbed oxygen in SBA-15 [21]. Figure 4c shows the high-resolution XPS spectrum of the Ni 2p region. The binding energies at around 853.4, 856.0, and 860.1 eV are attributed to the Ni 2p 3/2 peaks, and the 872.2 and 878.7 eV peaks are attributed to the Ni 2p 1/2 peaks, all of which suggests that the oxidation state of Ni is 2⁺ in sample 30 % NiO/ZnO/SBA-15 [22, 23]. In Fig. 4d, the peaks around 1021.9 and 1045.0 eV are attributed to the Zn 2p^{3/2} and Zn 2p^{1/2}, indicating the normal oxidation state of Zn²⁺ for our sample [24, 25]. All of the XPS results confirm the successful introduction of NiO and ZnO particles in the channels of SBA-15.

Nitrogen adsorption-desorption isotherms were used to characterize the surface area as well as porosity of samples SBA-15, 20 % NiO/ZnO/SBA-15, 30 % NiO/ZnO/SBA-15, and 40 % NiO/ZnO/SBA-15, and the results are shown in Fig. 5. The isotherms of these four samples show the same type IV isotherm model with a H1-type hysteresis loop, suggesting that all of them are mesoporous materials with two-dimensional hexagonal structures [19]. No obvious changes are detected in the isotherm type, suggesting that ordered mesoporous channels of SBA-15 are well kept after the loading of NiO and ZnO nanoparticles, coincident with the results from the above LAXRD and TEM analysis. Physico-chemical parameters of the samples are summarized in Table 1. Clearly, with the increase of NiO and ZnO loading, BET surface area, pore diameter, and pore volume of the samples decrease. In addition, the inflection point of the capillary condensation step on the isotherm shifts to a lower relative pressure with increasing NiO and ZnO loading, suggesting the reduction of mesopore size, which indirectly confirms the existence of NiO and ZnO nanoparticles in the channels of SBA-15.



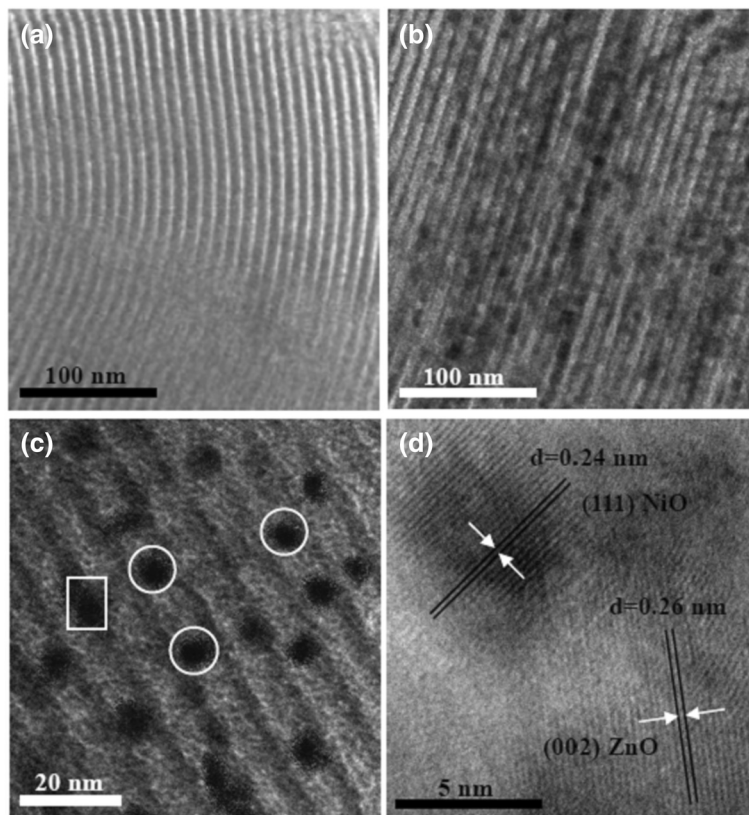


Fig. 3 TEM images of SBA-15 and 30 % NiO/ZnO/SBA-15. **a** SBA-15. **b** lower-magnification TEM image of 30 % NiO/ZnO/SBA-15. **c** Higher-magnification TEM image of 30 % NiO/ZnO/SBA-15. **d** HRTEM of 30 % NiO/ZnO/SBA-15

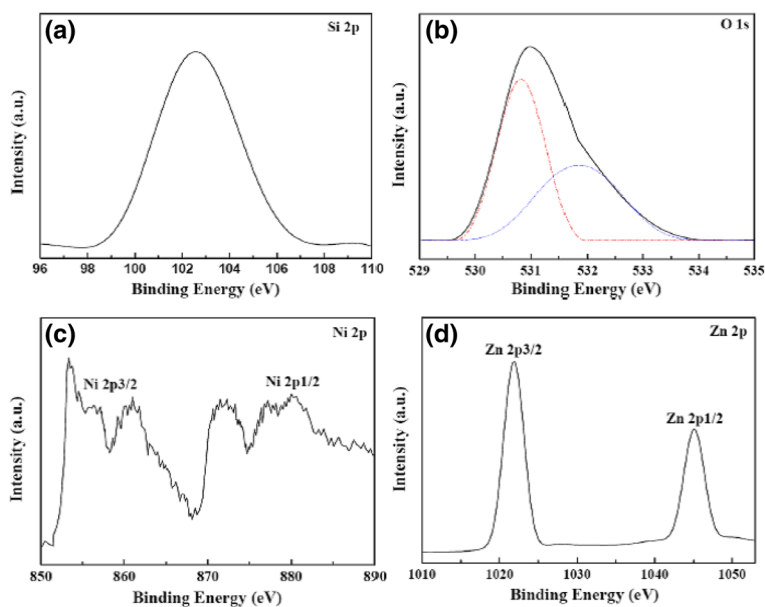


Fig. 4 XPS spectra of 30 % NiO/ZnO/SBA-15. **a** Si 2p. **b** O 1 s. **c** Ni 2p. **d** Zn 2p

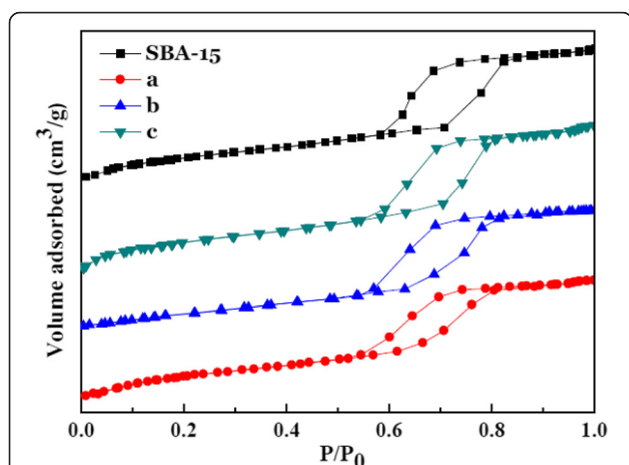


Fig. 5 Nitrogen physisorption isotherms of SBA-15 and NiO/ZnO/SBA-15 nanocomposites with different NiO/ZnO loading: (a) 20 % NiO/ZnO/SBA-15, (b) 30 % NiO/ZnO/SBA-15, and (c) 40 % NiO/ZnO/SBA-15

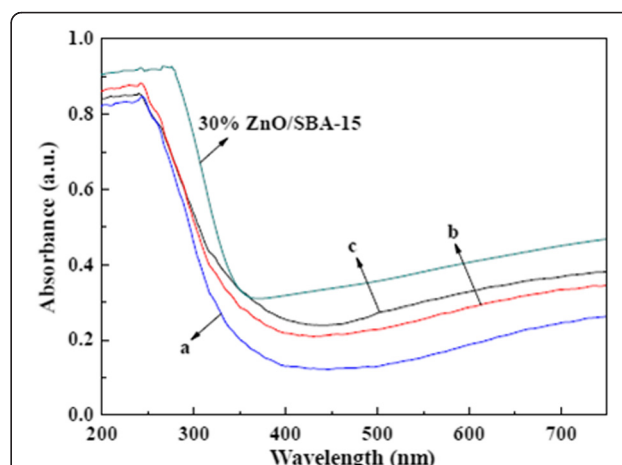


Fig. 6 UV-vis absorption spectra of 30 % ZnO/SBA-15 and NiO/ZnO/SBA-15 nanocomposites with different NiO/ZnO loading: (a) 20 % NiO/ZnO/SBA-15, (b) 30 % NiO/ZnO/SBA-15, and (c) 40 % NiO/ZnO/SBA-15

UV-vis spectra of NiO/ZnO/SBA-15 samples with different NiO and ZnO loading are shown in Fig. 6. Clearly, with the increase of NiO and ZnO loading, the absorption band edge shows a red-shift, which can be ascribed to the well-known quantum size effect based on the above XRD analysis and TEM image of crystalline size [26]. Moreover, compared with 30 % ZnO/SBA-15, the absorption band edges of samples extend greatly toward ultraviolet light regime.

Photocatalytic Measurements on NiO/ZnO/SBA-15 Nanocomposites

To evaluate the photocatalytic activity of the as-prepared NiO/ZnO/SBA-15 nanocomposites, the photodegradation of the well-known organic MO, a typical pollutant in the textile industry, was investigated in water under UV irradiation, and the experimental results are shown in Fig. 7. As an industry standard, Degussa P-25 was chosen for the comparative study. Sample 20 % NiO/ZnO/SBA-15 was used to test the adsorption ability without UV irradiation. As can be seen in Fig. 7, during the initial 30 min, due to

the adsorption of MO on the surface of sample 20 % NiO/ZnO/SBA-15, the concentration of MO rapidly decreases and about 50.8 % of MO decolors. After that, the concentration of MO is kept unchanged, suggesting the equilibrium between the adsorption and desorption of MO is achieved. In the absence of UV irradiation, samples 20 % NiO/ZnO/SBA-15, 30 % NiO/ZnO/SBA-15, and 40 % NiO/ZnO/SBA-15 exhibit a much better adsorption capability of MO than that of commercial P-25, which mainly results from their much larger specific surface area and pore volumes. Moreover, 20 % NiO/ZnO/SBA-15 shows higher adsorption capacity of 50.8 % for MO than that of 30 % NiO/ZnO/SBA-15 and 40 % NiO/ZnO/SBA-15 for its highest specific surface area and pore volumes (as shown in Table 1).

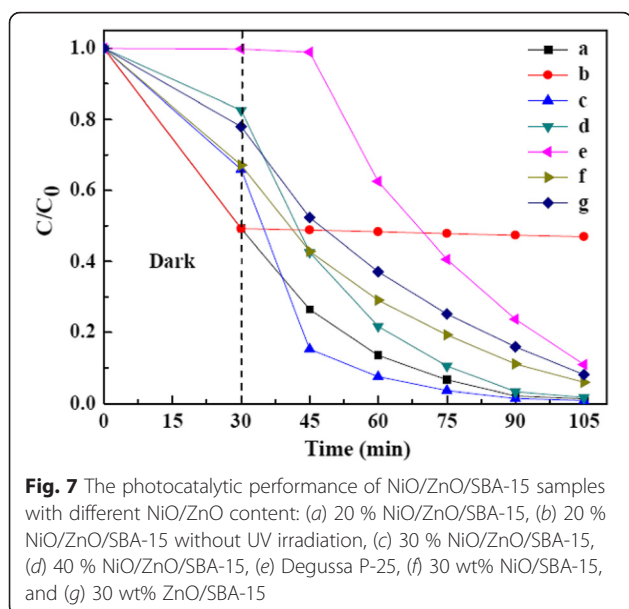
Based on Langmuir-Hinshelwood kinetics, the rate constants of photodecomposition of MO can be evaluated by the formula [27]:

$$\ln(C_0/C) = kt, \quad (1)$$

where C_0 is the initial concentration of the MO solution, C is the concentration of the MO solution, k is a rate constant, and t is the reaction time. After a simple calculation, the values of k are 0.0484, 0.0588, 0.0518, 0.0295, 0.0324, and 0.0302 min^{-1} for sample 20 % NiO/ZnO/SBA-15, 30 % NiO/ZnO/SBA-15, 40 % NiO/ZnO/SBA-15, Degussa P-25, 30 % ZnO/SBA-15, and 30 % NiO/SBA-15, respectively. The results show that NiO/ZnO/SBA-15 nanocomposites have better photocatalytic activities than Degussa P-25, and three factors are believed to account for their better photocatalytic activities. Firstly, the large specific surface areas of NiO/ZnO/SBA-15 nanocomposites are beneficial to the adsorption of MO molecules [28]. Secondly, ordered microporous network

Table 1 Physicochemical parameters derived from nitrogen physisorption and XRD data for different samples (d_{100} is the interplanar spacing of the hexagonal structure; a_0 represents the pore-to-pore distance of the hexagonal structure)

Samples	d_{100} (nm)	a_0 (nm)	S_{BET} (m^2/g)	Pore diameter (nm)	Pore volume (cm^3/g)
S0	10.6	12.2	812.5	6.43	0.98
S1	9.9	11.4	698.1	6.19	0.89
S2	10.1	11.7	584.8	6.13	0.80
S4	10.3	11.9	509.3	6.06	0.73



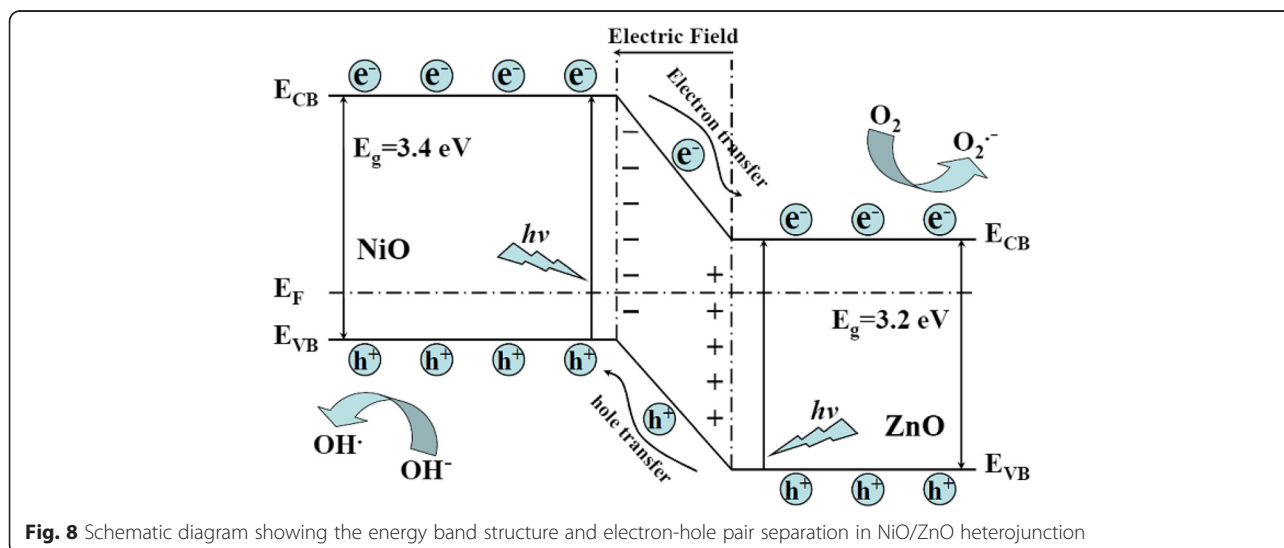
of NiO/ZnO/SBA-15 nanocomposites can help to promote diffusion and transportation of oxygen species and MO molecules, which greatly enhance photocatalytic activity by facilitating access to reactive sites of NiO/ZnO [29]. Lastly, the NiO/ZnO heterojunction in NiO/ZnO/SBA-15 nanocomposites can improve the separation rate of photogenerated electrons and holes, which reduce the recombination rates and hence improve the photocatalytic activity. Among the three samples of NiO/ZnO/SBA-15 nanocomposites, sample 20 % NiO/ZnO/SBA-15 possesses the lowest k value (0.0484 min^{-1}), higher than that of 30 % ZnO/SBA-15 (0.0324 min^{-1}) and 30 % NiO/SBA-15 (0.0302 min^{-1}), which support that the NiO/ZnO heterojunction plays an important role in the improvement of photocatalytic activity. Figure 8 shows the proposed

energy band structure diagram of NiO/ZnO heterojunction. The valence band (VB) and conduction band (CB) of ZnO are lower than that of NiO. When the heterojunction is excited by solar light, the photogenerated electron will be transferred from the CB of NiO to the CB of ZnO. Conversely, the photogenerated hole can be transferred from the VB of ZnO to the CB of NiO, indicating that the photogenerated electrons and holes are efficiently separated [30].

Compared with sample 20 % NiO/ZnO/SBA-15 ($k = 0.0484 \text{ min}^{-1}$) and 40 % NiO/ZnO/SBA-15 ($k = 0.0518 \text{ min}^{-1}$), sample 30 % NiO/ZnO/SBA-15 shows the highest photocatalytic activity ($k = 0.0588 \text{ min}^{-1}$), suggesting that there is an optimal loading dosage of NiO/ZnO nanoparticles. In fact, with the decrease of NiO/ZnO loading, the adsorption of NiO/ZnO/SBA-15 nanocomposites becomes increased and the size of NiO/ZnO nanoparticles is decreased. As well known, a higher adsorption is beneficial to the improvement of photoactivity, while smaller nanoparticles in the pore channels of SBA-15 will increase the distance between photoactive sites and the adsorption sites at the surface and enhance the recombination rate of photoinduced electron-hole pairs.

Conclusions

In summary, NiO/ZnO/SBA-15 nanocomposites with different NiO/ZnO loading were successfully fabricated by using a two-solvent method. The photocatalytic measurement results indicated that the as-obtained NiO/ZnO/SBA-15 nanocomposites possessed higher photocatalytic activity than Degussa P-25 for the degradation of MO dye under UV light irradiation. Higher adsorption performance and enhanced separation efficiency of photogenerated electron-hole pairs are believed to be responsible for the



great enhancement of photocatalytic activity. Moreover, there exists an optimal loading of NiO/ZnO for NiO/ZnO/SBA-15 nanocomposites in terms of photocatalytic activity, which is dependent of the adsorption of nanocomposites and NiO/ZnO nanoparticles sizes.

Competing interests

The authors declare that they have no competing interests.

Authors' contributions

TTY performed the synthesis and the structure study of samples and analyzed the data. ZMB performed the investigations of photocatalytic properties and analyzed the obtained data. PD and XXY contributed in the drafting and revision of the manuscript. PD and MZW supervised the work and finalized the manuscript. All authors read and approved the final manuscript.

Acknowledgements

This work was financed by the 211 project of Anhui University, National Natural Science Foundation of China (11374013, 51502002, 11404001, 61290301), Provincial Science Foundation of Anhui (1608085ME97), Outstanding young talent fund of Anhui Province (J05201424), and Research Fund for the Doctoral Program of Higher Education of China (20133401110002).

Author details

¹Key laboratory of Information Materials and Device, School of Physics and Materials Science, Anhui University, Hefei 230039, People's Republic of China.

²Engineering Technology Research Center of Magnetic Materials, Hefei 230039, People's Republic of China.

Received: 20 January 2016 Accepted: 19 April 2016

Published online: 27 April 2016

References

- Osterloh FE (2013) Inorganic nanostructure for photoelectrochemical and photocatalytic water splitting. *Chem Soc Rev* 42:2294–320
- Wang HL, Zhang LS, Chen ZG, Hu JQ, Li SJ, Wang ZH et al (2014) Semiconductor heterojunction photocatalysts: design, construction, and photocatalytic performances. *Chem Soc Rev* 43:5234–44
- Xu XJ, Hu LF, Gao N, Liu SX, Wageh S, Al-Ghamdi AA et al (2015) Controlled growth from ZnS nanoparticles to ZnS-CdS nanoparticle hybrids with enhanced photoactivity. *Adv Funct Mater* 25:445–454
- Zhang XY, Qin JQ, Xue YN, Yu PF, Zhang B, Wang LM et al (2014) Effect of aspect ratio and surface defects on the photocatalytic activity of ZnO nanorods. *Sci Rep* 4:4596
- Hong Y, Tian CG, Jiang BJ, Wu AP, Zhang Q, Tian GH et al (2013) Facile synthesis of sheet-like ZnO assembly composed of small ZnO particles for highly efficient photocatalysis. *J Mater Chem A* 1:5700–8
- Weng B, Yang MQ, Zhang N, Xu YJ (2014) Toward the enhanced photoactivity and photostability of ZnO nanospheres via intimate surface coating with reduced graphene oxide. *J Mater Chem A* 2:9380–9
- Kumar SG, Rao KSRK (2015) Zinc oxide based photocatalysts: tailoring surface-bulk structure and related interfacial charge carrier dynamics for better environmental applications. *RSC Adv* 5:3306–51
- Su CY, Yang TH, Gurylev V, Huang SH, Wu JM, Perng TP (2015) Extremely high efficient nanoreactor with Au@ZnO catalyst for photocatalysis. *Nanotechnol* 26:394001
- Tian FS, Liu YL (2013) Synthesis of p-type NiO/n-type ZnO heterostructure and its enhanced photocatalytic activity. *Scripta Mater* 69:417–9
- Zhang ZY, Shao CL, Li XH, Wang CH, Zhang MY, Liu YC (2010) Electrospun nanofibers of p-type NiO/n-type ZnO heterojunctions with enhanced photocatalytic activity. *ACS Appl Mater Inter* 2:2915–23
- Li JN, Zhao F, Zhang L, Zhang MY, Jiang HF, Li S et al (2015) Electrospun hollow ZnO/NiO heterostructures with enhanced photocatalytic activity. *RSC Adv* 5:67610–6
- Luo CZ, Li DL, Wu WH, Zhang YP, Pan CX (2014) Preparation of porous micro-nano-structure NiO/ZnO heterojunction and its photocatalytic property. *RSC Adv* 4:3090–5
- Imperor-Clerc M, Bazin D, Appay MD, Beauvier P, Davidson A (2004) Crystallization of beta-MnO₂ nanowires in the pores of SBA-15 silicas: in situ investigation using synchrotron radiation. *Chem Mater* 16:1813–21
- Van Der Meer J, Bardez-Giboire I, Mercier C, Revel B, Davidson A, Denoyel R (2010) Mechanism of metal oxide nanoparticle loading in SBA-15 by the double solvent technique. *J Phys Chem C* 114:3507–15
- Sun X, Yu HX, Zheng D, Wang XS, Li JS, Wang LJ (2013) Incorporation of nanoscale zero-valent iron particles inside the channels of SBA-15 silica rods by a "two solvents" reduction technique. *Appl Surf Sci* 279:1–6
- Zhao DY, Feng JL, Huo QS, Melosh N, Fredrickson GH, Chemka BF et al (1998) Triblock copolymer syntheses of mesoporous silica with periodic 50 to 300 angstrom pores. *Science* 279:548–52
- Lu QS, Wang ZY, Li JG, Wang PY, Ye XL (2009) Structure and photoluminescent properties of ZnO encapsulated in mesoporous silica SBA-15 fabricated by two-solvent strategy. *Nanoscale Res Lett* 4:646–654
- Aronson BJ, Blanford CF, Stein A (1997) Solution-phase grafting of titanium dioxide onto the pore surface of mesoporous silicates: synthesis and structural characterization. *Chem Mater* 9:2842–2851
- George J, Shylesh S, Singh AP (2005) Vanadium-containing ordered mesoporous silicas: Synthesis, characterization and catalytic activity in the hydroxylation of biphenyl. *Appl Catal A* 290:148–58
- Chen SF, Zhao W, Liu W, Zhang SJ (2009) Preparation, characterization and activity evaluation of p-n junction photocatalyst p-NiO/n-ZnO. *J Sol-gel Sci Techn* 50:387–96
- Chen SF, Zhang SJ, Liu W, Zhao W (2008) Preparation and activity evaluation of p-n junction photocatalyst NiO/TiO₂. *J Hazard Mater* 155:320–6
- Biju V (2007) Ni 2p X-ray photoelectron spectroscopy study of nanostructured nickel oxide. *Mater Res Bull* 42:791–6
- Zhao B, Ke XK, Bao JH, Wang CL, Dong L, Chen YW et al (2009) Synthesis of flower-like NiO and effects of morphology on its catalytic properties. *J Phys Chem C* 113:14440–7
- Liu YC, Zhong MY, Shan GY, Li YJ, Huang BQ, Yang GL (2008) Biocompatible ZnO/Au nanocomposites for ultrasensitive DNA detection using resonance Raman scattering. *J Phys Chem B* 112:6484–9
- Myung Y, Jang DM, Sung TK, Sohn YJ, Jung GB, Cho YJ et al (2010) Composition-tuned ZnO-CdSe core-shell nanowire arrays. *ACS Nano* 4:3789–800
- Volokitin Y, Sinzig J, de Jongh LJ, Vargaftik MN, Moiseevii II (1996) Quantum-size effects in the thermodynamic properties of metallic nanoparticles. *Nature* 384: 621–3
- Yang J, Zhang J, Zhu LW, Chen SY, Zhang YM, Tang Y et al (2006) Synthesis of nano titania particles embedded in mesoporous SBA-15: characterization and photocatalytic activity. *J Hazard Mater* 137:952–8
- Turchi CS, Ollis DF (1990) Photocatalytic degradation of organic water contaminants: mechanisms involving hydroxyl radical attack. *J Catal* 122:178–92
- Kruk M, Jaroniec M, Chang HK, Ryoo R (2000) Characterization of the porous structure of SBA-15. *Chem Mater* 12:1961–8
- Liu RL, Huang YX, Xiao AH, Liu HQ (2010) Preparation and photocatalytic property of mesoporous ZnO/SnO₂ composite nanofibers. *J Alloy Compd* 503:103–10

Submit your manuscript to a SpringerOpen® journal and benefit from:

- Convenient online submission
- Rigorous peer review
- Immediate publication on acceptance
- Open access: articles freely available online
- High visibility within the field
- Retaining the copyright to your article

Submit your next manuscript at ► springeropen.com